Valley polarization dependence of nonreciprocal transport in a chiral semiconductor

Kenta Sudo,[1] Yuki Yanagi,[2] Takeshi Takahashi,[3] Kim-Khuong Huynh,[4] Katsumi Tanigaki [®],[5]
Kaya Kobayashi [®],[3,6] Michi-To Suzuki,[1,7] and Motoi Kimata [®][1,*]

[1]*Institute for Materials Research, Tohoku University, Sendai, Miyagi, Japan*
[2]*Liberal Arts and Sciences, Toyama Prefectural University, Imizu, Toyama 939-0398, Japan*
[3]*Department of Physics, Okayama University, Okayama, Japan*
[4]*AIMR, Tohoku University, 1-1-2 Katahira, Aoba, Sendai 980-8577, Miyagi, Japan*
[5]*BAQIS, Bld. 3, No.10 Xibeiwang East Rd., Haidian District, Beijing 100193, China*
[6]*Research Institute for Interdisciplinary Science, Okayama University, Okayama, Japan*
[7]*Center for Spintronics Research Network, Graduate School of Engineering Science, Osaka University,
Toyonaka, Osaka 560-8531, Japan*

We report that the strong spin-valley coupling in chiral tellurium can modify the electronic structures, and how it dominates the nonreciprocal transport. The observed nonreciprocal magnetoresistance shows anomalous suppression in high magnetic fields. This behavior contradicts the linearity of nonreciprocal signals to the fields observed in other materials. We find that the magnetic field-induced fully valley polarized states in tellurium trigger the deviation from the linearity. Our results establish the essential role of the valley degree of freedom for the cross-correlation phenomena in chiral materials, in addition to the previously discussed spin-charge coupling.

The absence of inversion symmetry in condensed matter physics usually has intriguing consequences. Many important phenomena with a wide range of applications, such as piezoelectricity, ferroelectricity, and optical activity, appear only in both polar and chiral noncentrosymmetric insulating crystals. The recent studies of noncentrosymmetric materials have become even more interesting thanks to the understanding of cross correlation between spins and conduction electrons. Among a variety of noncentrosymmetric conductors, chiral conductors, of which the spatial inversion symmetry is broken by the various types of chiral order such as structural, magnetic, and electronic origins, have been attracting wide attention due to their characteristic physical properties [1–3]. The electronic structures of chiral materials are particularly studied since the unique cross-correlation functionalities, such as the chirality-induced spin selectivity (CISS) effect [4–9] and nonreciprocal transport under a magnetic field [4,10–14], originate in the lack of inversion symmetry. The former effect enables us to generate spin polarization by external current without magnetic elements, and the latter realizes a magnetic-field-controllable rectification of charge current without *p-n* junctions. In these phenomena, the chirality-mediated cross correction between spin and charge degrees of freedom through the spin orbit interaction, that is, the spin-charge coupling, plays an essential role.

The valley is another degree of freedom playing an important role in the electronic structures, which is characterized by multiple local extrema of band structure with degenerated energy in the momentum space [15–17]. The valley degree

of freedom is especially crucial in two-dimensional (2D) materials, and is the indispensable ingredient for valleytronics, in which the valley dependent physical properties, such as the control of optical polarization, valley transport and Hall effects, and valley Zeeman effect, are intensively studied [18–20]. However, the importance of the valley is limited to 2D materials, and no perspective is given in bulk chiral materials. Thus, integrating the degree of freedom of the valley with a chiral material will produce rich functionalities based on multiple (spin, charge, and valley) degrees of freedom. However, to date, the valley degree of freedom has not been manifested in chiral cross-correlation responses.

In this study, we show the magnitude of the nonreciprocal magnetoresistance (MR) of chiral tellurium (Te), and how it strongly depends on the polarization of the valley degree of freedom: the nonreciprocal MR is anomalously suppressed when the valley in Te is polarized. This finding is in contrast with the previously studied chiral cross-correlation responses, which are only related to the spin. We also found that the spin-valley coupling of Te has a different symmetry compared with that of 2D materials. Therefore, our results expand the physics of cross correlations in chiral materials and also the material developments for valleytronics.

Bulk elemental Te [Fig. 1(a)], which is the focus of this study, is a nonmagnetic semiconductor with a chiral structure. The electronic band structure of Te has a double maximum valence band near the H point in momentum (k) space. Figure 1(b) shows the semiempirical band structure of Te [21–28]. Owing to the symmetry-broken chiral structure and spin-orbit interaction, the band structure of Te is spin polarized [24,25,29]. The spin-polarized direction is radial from the H point, and this spin texture is entirely different from the helical spin texture in polar Rashba systems [29,30]. The
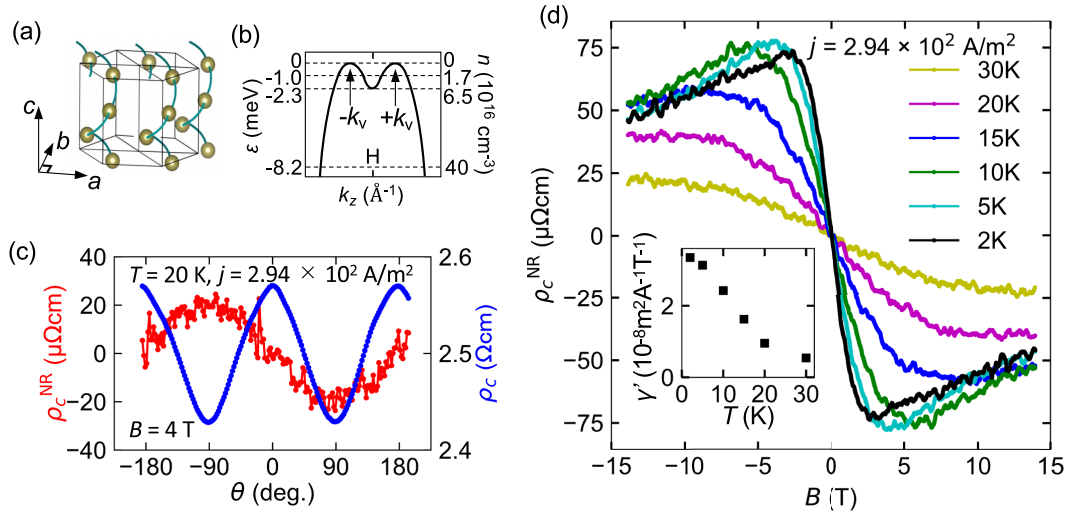
*motoi.kimata.b4@tohoku.ac.jp

FIG. 1. (a) Schematic of the crystal structure of elemental Te. (b) Solid line is schematic semiempirical valence band structure near the *H* point [22]. Dashed lines exhibit energy levels with various E_F from the top of the valence band. Corresponding values of n are also shown in the right axis. (c) Angular dependence of ρ_c (right axis) and ρ_c^{NR} (left axis) for $B = 4$ T and $T = 20$ K. In such low-field and high-temperature conditions, Zeeman energy for spin-polarized valley is smaller than the thermal broadening of Fermi level. (d) Main panel: Magnetic field dependence of ρ_c^{NR} at different temperatures. Inset: Temperature dependence of γ' extracted from the low-field slope of ρ_c^{NR}.

Fermi surface (FS) shape depends on the Fermi energy (E_F) from the top of the valence band. In addition, E_F is related to the hole carrier density (n) [Fig. 1(b)]. When n is above 6.5×10^{16} cm^{-3}, a single dumbbell-like FS is formed, and the radial spin texture on the single FS is observed by the angle-resolved photoemission spectroscopyexperiment [31]. In contrast, the single FS splits into two small pockets for $n < 6.5 \times 10^{16}$ cm^{-3} [22], indicating that the valley degree of freedom additionally appears in Te with small n. Notably, these valleys have spin polarization in the opposite direction, and thus can contribute to the emergence of unconventional cross-correlation responses originating from the spin-polarized valley, which has not been acknowledged in chiral cross correlations.

The *c*-axis resistivities (ρ_c) of the present crystals are semiconducting below room temperature [32]. The low-temperature Hall resistivity measurement indicated the presence of hole carriers for all measured crystals, and n was almost constant at low temperatures except for a slight reduction with temperature [32]. The values of n are estimated to be $\sim 10^{15}$–10^{16} cm^{-3} for distinct three samples, suggesting the presence of two small FS pockets for the present crystals. The holelike carriers at low density ($\sim 10^{15}$–10^{16} cm^{-3}) often present even in pure Te crystals, and their origin is unclear [33]. Despite the small carrier number, our Seebeck measurement (Fig. S1(c) of the Supplemental Material [32]) indicates that small FSs still exist.

The nonreciprocal MR, which is the difference in MR depending on the current polarity, is a recently observed transport phenomenon in noncentrosymmetric conductors, such as polar semiconductors [34], and chiral conductors [4,12–14]. In those reports, the magnitude of the nonreciprocal MR is maximized when the magnetic field is parallel to the spin direction, whose momentum (k) is parallel to the external current, and is proportional to the magnetic field strength. These features can be understood by the magnetic-field-induced dis-

tortion of the spin-polarized band by the Zeeman effect [34], where the spin-charge coupling in the *k* space is critical.

Figure 1(c) shows the angular dependence of ρ_c and the nonreciprocal resistivity (ρ_c^{NR}) for $B = 4$ T and $T = 20$ K for sample 1. Under these conditions, the thermal energy $k_B T$ ($= 1.63$ meV) of the measured temperature (20 K) is larger than E_F (~ 0.4 meV) and the difference in the Zeeman energy for the spin-polarized valley (~ 0.8 meV). Here, the definition of ρ_c^{NR} is expressed as $\rho_c^{NR} \equiv R^{2\omega} S/l$ with sample cross section S, and the distance of voltage contacts l. $R^{2\omega}$ is the second harmonic resistance obtained from the lock-in 2ω method, and corresponds to the nonreciprocal resistance [34]. The magnetic field was rotated in the *bc* plane of the crystal and the field angle θ was measured from the *b* axis. As shown in Fig. 1(c), the ρ_c shows a twofold symmetric behavior consistent with the expected dependence of the longitudinal and transverse MR, that is, the ρ_c is large for $B \perp I$ ($\theta = 0°$) and small for $B \parallel I$ ($\theta = \pm 90°$). On the other hand, the ρ_c^{NR} shows onefold symmetry and reaches the maximum (minimum) when the magnetic field is parallel (antiparallel) to the *c* axis. This angular dependence of ρ_c^{NR} is consistent with the symmetry of the radial spin texture, where the spin polarization along the current direction (k_z) is parallel to the *c* axis.

Figure 1(d) shows the field dependence of ρ_c^{NR} for $\theta = 90°$ at various temperatures. In particular, for low-temperature data such as 2 K, ρ_c^{NR} shows linear dependence in low fields of $B < \sim 2$ T, and is then suppressed at higher fields. This characteristic field dependence is different from the previous reports, including chiral conductors, where the magnitude of the nonreciprocal MR shows monotonic linear field dependence [12–14,34,35]. The previously reported linear field dependence of ρ_c^{NR} was attributed to a small Zeeman shift of the spin-polarized FS. Thus, if the FS is largely changed by a magnetic field, the nonreciprocal MR may exhibit unconventional responses to magnetic fields. The characteristic
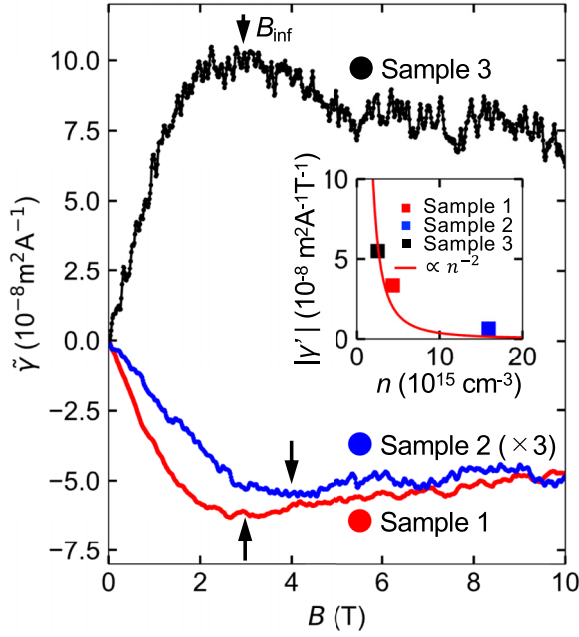
FIG. 2. Main panel: Magnetic field dependence of $\tilde{\gamma}$ for distinct samples. Inset: n dependence of $|\gamma'|$ for three samples obtained from low-field linear region of $\tilde{\gamma}$, that is, $\tilde{\gamma} = \gamma'B$.
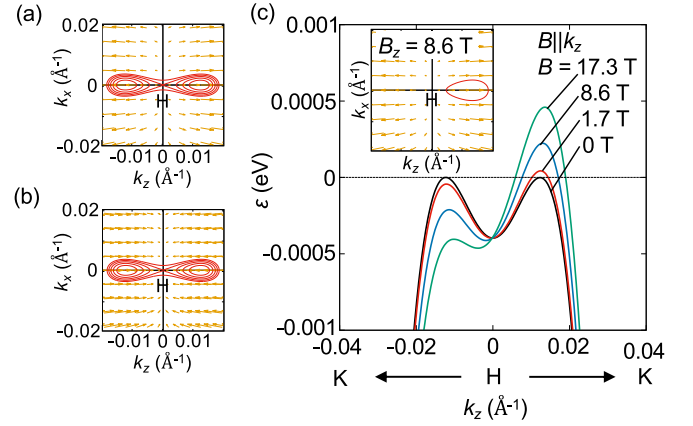

FIG. 3. (a),(b) Spin texture of the top of the valence bands for right-handed and left-handed Te crystals in the k_x-k_z plane, respectively. The sign of spin texture is inverted depends on the crystal chirality. The direction of spin is indicated by orange arrows. Solid red lines show FS cross section with various E_F. (c) Main panel: Magnetic field evolution of spin-polarized band in Te for $B||c$ obtained from the first-principles calculations. Inset: Spin texture for $B = 8.6$ T near the H point obtained from the first-principles calculations (orange arrows). The spin texture is mostly not affected by the external magnetic field in such field range. Ellipsoidal solid line is FS for $E_F = -0.2$ meV. Only the single FS is observed at high magnetic valley polarized state. The Zeeman effect only for spin moment is considered in this calculation.

feature of field-dependent ρ_c^{NR} becomes less prominent as the temperature increases, indicating that the increase in thermal energy competes with the origin of this behavior.

The inset of Fig. 1(d) shows the temperature dependence of γ' [$\equiv \rho_c^{NR}/(\rho_c jB)$]. This parameter is a coefficient of ρ_c^{NR} normalized by ρ_c and j (current density) to measure the magnitude of the nonreciprocal response, which is extracted from the linear slope of ρ_c^{NR} in the low-field region. In this region, the expression of $\rho_c^{NR} = \rho_c j\gamma'B$ is valid because $\rho_c^{NR} \propto B$. As shown in the inset, γ' monotonously increases as the temperature decreases, and this behavior can be reasonably explained by the temperature dependence of resistivity, which is roughly proportional to n^{-2} as discussed in Ref. [34].

We also measured the nonreciprocal MR of distinct samples with different n values, as shown in Fig. 2. Since the nonreciprocal MR of this material does not follows B-linear dependence, a modified coefficient $\tilde{\gamma}$ was used, which corresponds to $\gamma'B$ in the expression of $\rho_c^{NR} = \rho_c j\gamma'B$ as a measure of magnitude of nonreciprocal MR for different samples, that is, $\rho_c^{NR} = \rho_c j\gamma'B = \rho_c j\tilde{\gamma}$. The main panel in Fig. 2 shows the field dependence of $\tilde{\gamma}$ for samples 1–3 at 2 K. Note that only sample 3 shows the opposite sign of $\tilde{\gamma}$ compared with other samples. This sign change likely originates from the opposite crystal chirality of sample 3 compared to samples 1 and 2. As can be seen in the main panel of Fig. 2, all the samples show the same trend in the field dependence, indicating that the characteristic field-dependent behavior of nonreciprocal MR in this material is intrinsic. In addition, $|\gamma'|$ extracted from the low-field linear slope is mostly proportional to n^{-2} (inset of Fig. 2), which is consistent with the standard behavior observed in the previous report [34]. Thus, this systematic observation of the unconventional behavior of ρ_c^{NR} indicates that the observed features originate from the bulk properties of the

measured crystals. Note that the values of $|\gamma'|$ for the present crystals (inset of Fig. 2, $n \approx 10^{16}$ cm^{-3}) are approximately four orders of magnitude larger than those in a previous report for BiTeBr ($n \approx 10^{18}$ cm^{-3}), and this enhancement is reasonably explained by the decrease in carrier density, that is, $\gamma' \propto\sim n^{-2}$ [34]. However, these samples show different field values for inflection of $\tilde{\gamma}$ (B_{inf}), as indicated by the arrows: B_{inf} shifts to higher fields for high-carrier-density crystals. These nonmonotonous field dependencies of ρ_c^{NR} cannot be explained by the simple conventional model, where the magnetic shift of the spin-polarized FS is a small perturbation to the Fermi wave vector. Thus, these results suggest a drastic change in FS in the magnetic field higher than B_{inf} for $B||c$.

To confirm the chirality-dependent sign reversal of nonreciprocal MR and the drastic change in FS suggested from the experimental results, we performed first-principles calculation of the band structure in the magnetic field for $B||c$ using the Vienna *ab initio* simulation (VASP) package and WANNIER90 code [36,37]. The details of calculation conditions are described in Ref. [32]. Figures 3(a) and 3(b) show the spin textures of right-handed and left-handed crystals, respectively, where the spin textures are inverted. Figure 3(c) shows the magnetic field evolution of the spin-polarized band structure and spin texture at $B = 8.6$ T for the right-handed crystal (inset). As the field increases, the asymmetry of the band structure is induced because the spin polarization is opposite to the H point. The Zeeman effect only for the spin moment is considered in this first principles calculation. In contrast to the case for $B||k_z$ [Fig. 3(c)], the spin-polarized band is mostly independent of the magnetic field when the magnetic field is perpendicular to the c axis [32], indicating that the
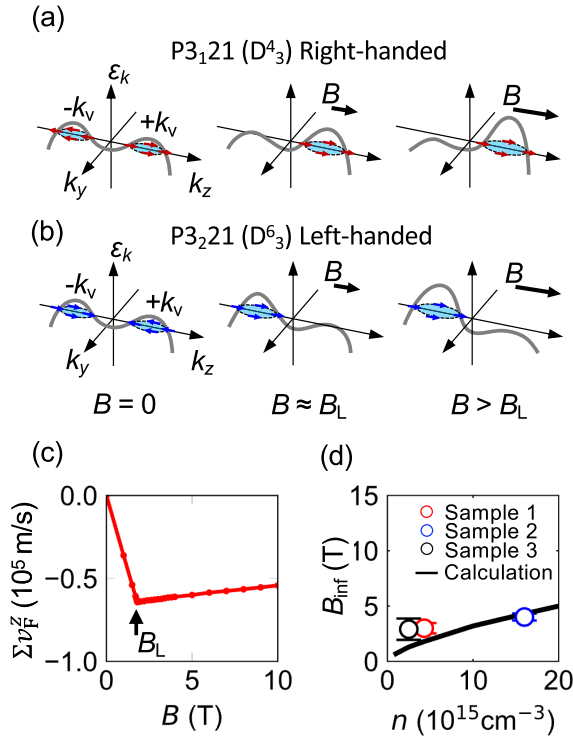
FIG. 4. (a),(b) Schematic illustrations of field evolution of spin-polarized band for *c*-axis magnetic field. Panels (a) and (b) represent the case for right-handed and left-handed crystals, respectively. Red arrows in (a) and blue arrows in (b) represent outward and inward spin textures for right- and left-handed crystals, respectively. When *n* is sufficiently small, the spin-polarized FS split into two distinct valleys as shown in the left figure. As the field increases, one of two valleys disappear when the Zeeman energy of spin-polarized valley exceeds E_F. Since the crystal chirality is opposite for (a) and (b), the excited valleys by magnetic field are also opposite. (c) Calculated field dependence of $\sum v_F^z$. E_F is set to -0.4 meV, which corresponds to *n* of sample 1 ($n \approx 4 \times 10^{15}$ cm^{-3}). (d) Experimentally obtained B_{inf} vs *n* for distinct samples (symbols). The solid line is obtained from the simulation based on the model calculation. In this model calculation, the Zeeman effect is considered for effective magnetic moment including spin and orbital moments.

large Zeeman effect is absent for $B \perp k_z$. As expected from this calculation, the Lifshitz transition (disappearance of one of the two FSs) occurs when the Zeeman energy of the spin-polarized FS exceeds E_F. The energy scale of valley obtained from our first principles calculations ($\sim$0.4 meV) is smaller than that estimated from experiments ($\sim$2.3–3 meV) [22,23]. Although the calculated energy scale of the valley varies from $\sim$0.3 to $\sim$2 meV depending on calculation methods [38–40], the formation of valley structure is widely confirmed for moderate spin-orbit coupling since the mechanism is based on the band mixing due to the spin-orbit coupling for the linearly crossing bands in the absence of spin-orbit interaction. The chirality-dependent spin texture determines the sign of nonreciprocal MR since the sign of spin texture is inverted depending on the crystal chirality. The position of the valley ($+k_v$ or $-k_v$) in the field-induced valley polarized state also depends on the crystal chirality as depicted in Figs. 4(a) and

4(b): the $+k_v$ ($-k_v$) valley is stabilized in the right-handed (left-handed) crystal at high magnetic fields.

To explain the nonmonotonous field dependence of ρ_c^{NR} based on the Lifshitz transition, we performed a model calculation of the nonreciprocal coefficient (which is defined as the sum of the Fermi velocities for positive and negative k_F under a magnetic field) with conventional semiempirical band parameters of Te near the *H* point, since the precise reproduction of the depth of valley structure in such a small energy is difficult in the current calculations as discussed above. In this model, we used the following band parameters with *k*-dependent spin polarization [21–28]:

$$\varepsilon(k_z) = Ck_z^2 + \sqrt{D^2k_z^2 + \Delta^2} - \Delta - E_0 \tag{1}$$

and

$$s_{eff}(k) = \left(\sim 0, \ \sim 0, \ \frac{3Dk_z}{2\sqrt{D^2k_z^2 + \Delta^2}}\right). \tag{2}$$

Here, $C = -36.7$ eV Å^2, $D = \pm 2.47$ eV Å (negative sign for right-hand structure $P3_121$, and positive for left-hand structure $P3_221$), $\Delta = 63$ meV, and $E_0 = 2.3$ meV are band parameters of Te, and s_{eff} is an effective spin including orbital moment [21–28]. Equation (2) indicates that the spin polarization mostly has a k_z component, in particular for small k_F [29,41,42]. This characteristic is consistent with the first-principles calculations of spin-polarized valleys (inset of Fig. 3). Consequently, the effective band structure under the *c*-axis magnetic field can be described as

$$\varepsilon(k_z) = Ck_z^2 + \sqrt{D^2k_z^2 + \Delta^2} - \Delta - E_0 + 2\mu_B s_{eff}(k_z)B. \tag{3}$$

When a weak magnetic field is applied along the k_z direction, the asymmetric band distortion is induced, as shown in Fig. 3, because the Zeeman term (final term) in Eq. (3) depends on the sign of k_z. By increasing the applied magnetic field, the difference in Zeeman energy at the local band maxima exceeds the E_F, and thus the Lifshitz transition occurs, as shown in Fig. 4(a). Subsequently, we will show the effect of Lifshitz transition on the nonreciprocal coefficient. The nonreciprocal MR is proportional to the asymmetry of the Fermi velocity at positive and negative k_F. We have calculated the sum of the Fermi velocities along the k_z direction (v_F^z) for each k_F using $v_F^z = \frac{1}{\hbar}\frac{\partial \varepsilon}{\partial k_z(k=k_F^z)}$ as a measure of nonreciprocal coefficient. k_F^z used here is determined by E_F obtained from *n* measured from the Hall coefficient.

Figure 4(b) shows the field dependence of the calculated nonreciprocal coefficient ($\sum v_F^z$) for E_F of -0.4 meV. This E_F value corresponds to sample 1, and determined by the relationship between *n* and E_F in Te [22]. As shown in Fig. 4(c), the absolute value of a nonreciprocal coefficient is proportional to the field strength in the low-field region for $B < B_L$; however, it decreases in higher fields. This behavior is consistent with the experimental observations at low temperatures, such as 2 K, as shown in the main panel of Fig. 2. Notably, one of the two valleys disappears at the peak field B_L in Fig. 4(a), that is, the Lifshitz transition occurs at the B_L. The decrease in ρ_c^{NR} above B_L can be explained as follows: For $B > B_L$, the E_F is only located at a single maximum of the valence band, and this band maximum is sharpened and becomes more

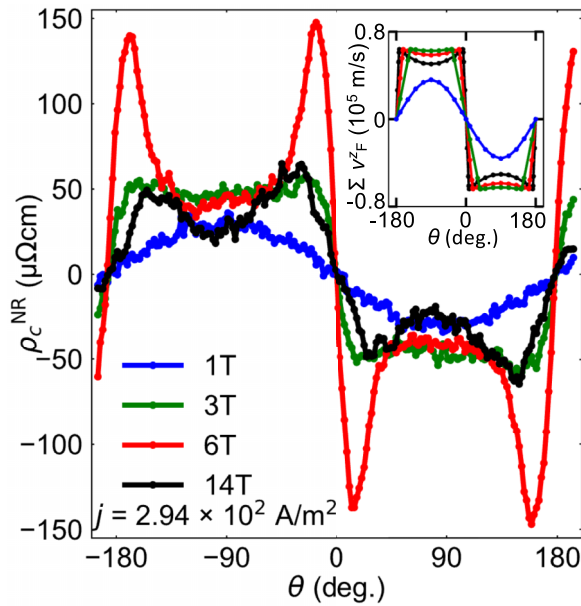FIG. 5. Main panel: Magnetic field evolution of angular dependence of ρ_c^{NR} at 2 K. For ρ_c^{NR}, nonmonotonous angular dependence was observed at high fields above 3 T. Inset: Simulated angular dependence of $\sum v_F^z$ for magnetic field strength of 1, 3, 6, and 14 T. The value of E_F is set to -0.4 meV corresponding to n of sample 1.

symmetric around the band maximum as the field increases. This leads to a reduction in ρ_c^{NR} when $B > B_L$. The symbols in Fig. 4(c) shows the experimentally obtained B_{inf} vs n for the three distinct samples. The solid line indicates the simulated n dependence of B_L, which is reasonably consistent with n dependence of B_{inf} from the experiment, indicating that the peak of the field-dependent ρ_c^{NR} originates from the Lifshitz transition of the spin-polarized valleys.

Finally, we discuss the unconventional field angle dependence of ρ_c^{NR}. The main panel of Fig. 5 shows the field variation of field-angle-dependent ρ_c^{NR} at 2 K. Similar to the case for $T = 20$ K, simple sinusoidal behavior was observed at 1 T. However, the shape of ρ_c^{NR} deviated from a sinusoidal curve when the field increased. In particular, at approximately $\theta = \pm 90°$, ρ_c^{NR} is suppressed, and a large hornlike feature is observed at 6 T in the intermediate angle between $B \perp c$ and $B \| c$. Furthermore, the amplitude of ρ_c^{NR} also shrinks for higher fields such as $B = 14$ T. This significant suppression of the amplitude in the angular dependence of ρ_c^{NR} can be qualitatively explained by the proposed model. The inset of Fig. 5 shows the calculated angular dependence of the nonreciprocal coefficient using the same model as in Fig. 4(b).

The value of E_F is set to -0.4 meV as similar to the previous calculation. In this model, when the magnetic field is tilted from the c axis, the Lifshitz transition occurs only when the c axis component of the external field (B_c) is larger than B_L. Thus, the nonreciprocal coefficient is suppressed in the angle region $|B_c| > |B_L|$, which is fulfilled when the magnetic field is close to the c axis. In addition, the nonreciprocal coefficient reaches a maximum at an intermediate angle, where $B_c = B_L$ is satisfied. However, the steep enhancement in ρ_c^{NR} observed at 6 T cannot be explained by our simple model. On the other hand, the amplitude of the field-angle-dependent ρ_c is monotonously increased as the field increases as shown in Ref. [32].

In this study, we found that the symmetry of spin-valley coupling in Te is different from that of conventional 2D materials [18–20], i.e., the spin polarization in 2D metal dichalcogenides is perpendicular to the plane [42], but that of Te is parallel to the chiral chain. Our finding will contribute to the expansion of material choices to establish various type of spin-valley responses with a wide variety of external fields configurations.

In conclusion, we investigated the nonreciprocal MR of bulk elemental Te, which is a simple nonmagnetic chiral semiconductor. The observed unconventional behavior of nonreciprocal MR is attributed to the Lifshitz transition of spin-polarized valleys near the H point. Cross correlations in chiral materials have been recently studied from the viewpoint of spin-charge coupling. In contrast, our present findings clearly show that the valley degree of freedom dominates the chiral cross-correlation responses in addition to the spin. We find that the symmetry of spin-valley configuration is unique compared with well-known 2D materials. Our results establish the importance of the valley degree of freedom in chiral materials and expand the chirality-mediated cross-correlation functionalities with multiple degrees of freedom.

[1] S.-H. Yang, Spintronics on chiral objects, Appl. Phys. Lett. **116**, 120502 (2020).

[2] S.-H. Yang, R. Naaman, Y. Paltiel, and S. S. P. Parkin, Chiral spintronics, Nat. Rev. Phys. **3**, 328 (2021).

[3] C. Guo, C. Putzke, S. Konyzheva, X. Huang, M. G.-Amigo, I. Errea, D. Chen, M. G. Vergniory, C. Felser, M. H. Fischer, T. Neupert, and P. J. W. Moll, Switchable chiral transport in charge-ordered kagome metal CsV$_3$Sb$_5$, Nature (London) **611**, 461 (2022).

[4] K. Shiota, A. Inui, Y. Hosaka, R. Amano, Y. Ōnuki, M. Hedo, T. Nakama, D. Hirobe, J.-I. Ohe, J.-I. Kishine, H. M. Yamamoto, H. Shishido, and Y. Togawa, Chirality-Induced Spin

Polarization Over Macroscopic Distances in Chiral Disilicide Crystals, Phys. Rev. Lett. **127**, 126602 (2021).

[5] R. Naaman and D. H. Waldeck, Chiral-induced spin selectivity effect, J. Phys. Chem. Lett. **3**, 2178 (2012).

[6] D. H. Waldeck, R. Naaman, and Y. Paltiel, The spin selectivity effect in chiral materials, APL Mater. **9**, 040902 (2021).

[7] R. Naaman, Y. Paltiel, and D. H. Waldeck, Chiral molecules and the electron spin, Nat. Rev. Chem. **3**, 250 (2019).

[8] R. Naaman, Y. Paltiel, and D. H. Waldeck, Chiral molecules and the spin selectivity effect, J. Phys. Chem. Lett. **11**, 3660 (2020).

[9] H. Shishido, R. Sakai, Y. Hosaka, and Y. Togawa, Detection of chirality-induced spin polarization over millimeters in polycrystalline bulk samples of chiral disilicides $NbSi_2$ and $TaSi_2$, Appl. Phys. Lett. **119**, 182403 (2021).

[10] T. Yokouchi, N. Kanazawa, A. Kikkawa, D. Morikawa, K. Shibata, T. Arima, Y. Taguchi, F. Kagawa, and Y. Tokura, Electrical magnetochiral effect induced by chiral spin fluctuations, Nat. Commun. **8**, 866 (2017).

[11] N. Jiang, Y. Nii, H. Arisawa, E. Saitoh, and Y. Onose, Electric current control of spin helicity in an itinerant helimagnet, Nat. Commun. **11**, 1601 (2020).

[12] G. L. J. A. Rikken and N. Avarvari, Strong electrical magnetochiral anisotropy in tellurium, Phys. Rev. B **99**, 245153 (2019).

[13] F. Calavalle, M. Suárez-Rodríguez, B. Martín-García, A. Johansson, D. C. Vaz, H. Yang, I. V. Maznichenko, S. Ostanin, A. Mateo-Alonso, A. Chuvilin, I. Mertig, M. Gobbi, F. Casanova, and L. E. Hueso, Gate-tuneable and chirality-dependent charge-to-spin conversion in tellurium nanowires, Nat. Mater. **21**, 526 (2022).

[14] D. Hirobe, Y. Nabei, and H. M. Yamamoto, Chirality-induced intrinsic charge rectification in a tellurium-based field-effect transistor, Phys. Rev. B **106**, L220403 (2022).

[15] A. Rycerz, J. Tworzydło, and C. W. J. Beenakker, Valley filter and valley valve in graphene, Nat. Phys. **3**, 172 (2007).

[16] K. Behnia, Polarized light boosts valleytronics, Nat. Nanotechnol. **7**, 488 (2012).

[17] C. E. Nebel, Electrons dance in diamond, Nat. Mater. **12**, 690 (2013).

[18] H. Zeng, J. Dai, W. Yao, D. Xiao, and X. Cui, Valley polarization in MoS_2 monolayers by optical pumping, Nat. Nanotechnol. **7**, 490 (2012).

[19] K. F. Mak, K. L. Mcgill, J. Park, and P. L. Muceuen, The valley Hall effect in MoS_2 transistors, Science **344**, 1489 (2014).

[20] A. Srivastava, M. Sidler, A. V. Allain, D. S. Lembke, A. Kis, and A. Imamoğlu, Valley Zeeman effect in elementary optical excitations of monolayer WSe_2, Nat. Phys. **11**, 141 (2015).

[21] O. Betbeder-Matibet and M. A. Hulin, Semi-empirical model for the valence band structure of tellurium, Phys. Status Solidi **36**, 573 (1969).

[22] E. Braun, L. J. Neuringer, and G. Landwehr, Valence band structure of tellurium from Shubnikov-de Haas experiments, Phys. Status Solidi **53**, 635 (1972).

[23] C. Guthmann and J. M. Thuillier, Fermi surface of tellurium, Phys. Status Solidi **38**, 635 (1970).

[24] T. Doi, K. Nakao, and H. Kamimura, The valence band structure of tellurium. I. The k·p perturbation method, J. Phys. Soc. Jpn. **28**, 36 (1970).

[25] K. Nakao, T. Doi, and H. Kamimura, The valence band structure of tellurium. III. The Landau levels, J. Phys. Soc. Jpn. **30**, 1400 (1971).

[26] E. L. Ivchenko and G. E. Pikus, Natural optical activity of semiconductors (tellurium), Fiz. Tverd. Tela (Leningrad) **16**, 1933 (1974) [Sov. Phys. Solid State **16**, 1261 (1975)].

[27] L. S. Dubinskaya and I. I. Farbshtein, Natural optical activity and features of the structure of the electronic energy spectrum of tellurium, Sov. Phys. Solid State **20**, 437 (1978).

[28] H. Stolze, M. Lutz, and P. Grosse, The optical activity of tellurium, Phys. Status Solidi **82**, 457 (1977).

[29] M. Hirayama, R. Okugawa, S. Ishibashi, S. Murakami, and T. Miyake, Weyl Node and Spin Texture in Trigonal Tellurium and Selenium, Phys. Rev. Lett. **114**, 206401 (2015).

[30] K. Ishizaka, M. S. Bahramy, H. Murakawa, M. Sakano, T. Shimojima, T. Sonobe, K. Koizumi, S. Shin, H. Miyahara, A. Kimura, K. Miyamoto, H. Namatame, M. Taniguchi, R. Arita, N. Nagaosa, K. Kobayashi, Y. Murakami, R. Kumai, Y. Kaneko *et al.*, Giant Rashba-type spin splitting in bulk BiTeI, Nat. Mater. **10**, 521 (2011).

[31] M. Sakano, M. Hirayama, T. Takahashi, S. Akebi, M. Nakayama, K. Kuroda, K. Taguchi, T. Yoshikawa, K. Miyamoto, T. Okuda, K. Ono, H. Kumigashira, T. Ideue, Y. Iwasa, N. Mitsuishi, K. Ishizaka, S. Shin, T. Miyake, S. Murakami, T. Sasagawa, and T. Kondo, Radial Spin Texture in Elemental Tellurium with Chiral Crystal Structure, Phys. Rev. Lett. **124**, 136404 (2020).

[32] See Supplemental Material at http://link.aps.org/supplemental/10.1103/PhysRevB.108.125137 for the details of experimental methods; basic properties of measured crystals containing temperature dependence of longitudinal resistivity, carrier density determined by the Hall effect, and Seebeck coefficient; details of first principles calculations; calculated field response of spin polarized valley for B ⊥ c; angle dependence of longitudinal resistivity. The Supplemental Material also contains references related to the details of first principles calculations. This includes references to G. Kresse and D. Joubert, Phys. Rev. B **59**, 1758 (1999); A. V. Krukau, O. A. Vydrov, A. F. Izmaylov, and G. E. Scuseria, J. Chem. Phys. **125**, 224106 (2006); S. S. Tsirkin, I. Souza, and D. Vanderbilt, Phys. Rev. B **96**, 045102 (2017); J. Paier, M. Marsman, K. Hummer, G. Kresse, I. C. Gerber, and J. G. Angyan, J. Chem. Phys. **124**, 154709 (2006).

[33] K. Takita, T. Hagiwara, and S. Tanaka, Galvanomagnetic effects in p-type tellurium at low temperatures. I, J. Phys. Soc. Jpn. **31**, 1469 (1971).

[34] T. Ideue, K. Hamamoto, S. Koshikawa, M. Ezawa, S. Shimizu, Y. Kaneko, Y. Tokura, N. Nagaosa, and Y. Iwasa, Bulk rectification effect in a polar semiconductor, Nat. Phys. **13**, 578 (2017).

[35] P. He, C.-H. Hsu, S. Shi, K. Cai, J. Wang, Q. Wang, G. Eda, H. Lin, V. M. Pereira, and H. Yang, Nonlinear magnetotransport shaped by Fermi surface topology and convexity, Nat. Commun. **10**, 1290 (2019).

[36] G. Kresse and J. Furthmüller, Efficient iterative schemes for ab initio total-energy calculations using a plane-wave basis set, Phys. Rev. B **54**, 11169 (1996).

[37] G. Pizzi, V. Vitale, R. Arita, S. Blügel, F. Freimuth, G. Géranton, M. Gibertini, D. Gresch, C. Johnson, T. Koretsune, J. Ibañez-Azpiroz, H. Lee, J.-M. Lihm, D. Marchand, A. Marrazzo, Y. Mokrousov, J. I. Mustafa, Y. Nohara, Y. Nomura, L. Paulatto *et al.*, Wannier90 as a community code: New

features and applications, J. Phys.: Condens. Matter **32**, 165902 (2020).

[38] H. Peng, N. Kioussis, and G. J. Snyder, Elemental tellurium as a chiral p-type thermoelectric material, Phys. Rev. B **89**, 195206 (2014).

[39] S. S. Tsirkin, P. A. Puente, and I. Souza, Gyrotropic effects in trigonal tellurium studied from first principles, Phys. Rev. B **97**, 035158 (2018).

[40] T. Ideue, M. Hirayama, H. Taiko, T. Takahashi, M. Murase, T. Miyake, S. Murakami, T. Sasagawa, and Y. Iwasa, Pressure-induced topological phase transition in noncentrosymmetric elemental tellurium, Proc. Natl. Acad. Sci. USA **116**, 25530 (2019).

[41] T. Furukawa, Y. Shimokawa, K. Kobayashi, and T. Itou, Observation of current-induced bulk magnetization in elemental tellurium, Nat. Commun. **8**, 954 (2017).

[42] T. Furukawa, Y. Watanabe, N. Ogasawara, K. Kobayashi, and T. Itou, Current-induced magnetization caused by crystal chirality in nonmagnetic elemental tellurium, Phys. Rev. Res. **3**, 023111 (2021).